Full Title：

Feasibility studies of radioiodinated pyridyl benzofuran derivatives as potential SPECT imaging agents for prion deposits in the brain

Running Title:

Pyridyl benzofurans as potential prion imaging agents

Takeshi Fuchigami[a]*, Masao Kawasaki[a], Hiroyuki Watanabe[b], Takehiro Nakagaki[c], Kodai Nishi[d], Kazunori Sano[e], Ryuichiro Atarashi[f], Mari Nakaie[a], Sakura Yoshida[a], Masahiro Ono[b], Noriyuki Nishida[c], Morio Nakayama[a]*

[a] Department of Hygienic Chemistry, Graduate School of Biomedical Sciences, Nagasaki University, 1-14 Bunkyo-machi, Nagasaki 852-8521, Japan

[b] Graduate School of Pharmaceutical Sciences, Kyoto University, 46-29 Yoshida Shimoadachi-cho, Sakyo-ku, Kyoto 606-8501, Japan.

[c] Department of Molecular Microbiology and Immunology, Graduate School of Biomedical Sciences, Nagasaki University, 1-12-4 Sakamoto, Nagasaki 852-8523, Japan

[d] Department of Radioisotope Medicine, Atomic Bomb Disease Institute, Nagasaki University, 1-12-4 Sakamoto, Nagasaki 852-8523, Japan

[e] Department of Physiology and Pharmacology, Faculty of Pharmaceutical Sciences, Fukuoka University, 8-19-1 Nanakuma, Jonan-ku, 814-0180, Fukuoka, Japan.

[f] Division of Microbiology, Department of Infectious Diseases, Faculty of Medicine, University of Miyazaki, 5200 Kiyotake-cho, Miyazaki, 889-1692, Japan.

*corresponding author:

Takeshi Fuchigami,

Graduate School of Biomedical Sciences, Nagasaki University, 1-14 Bunkyo-machi, Nagasaki 852-8521, Japan.

Tel.: +81-95-819-2442;

Fax: +81-95-819-2893;

E-mail: t.fuchigam@gmail.com

Morio Nakayama,

Graduate School of Biomedical Sciences, Nagasaki University, 1-14 Bunkyo-machi, Nagasaki 852-8521, Japan.

Tel.: +81-95-819-2441;

Fax: +81-95-819-2893;

E-mail: nakmorio@gmail.com

Abstract

Introduction: Prion diseases are fatal neurodegenerative disorders caused by the

deposition of abnormal prion protein aggregates (PrP^{Sc}) in the central nervous system.

This study aimed to evaluate the use of iodinated pyridyl benzofuran (IPBF) derivatives

as single-photon emission computed tomography (SPECT) probes for the detection of

cerebral PrP^{Sc} deposits.

Methods: *In vitro* binding assays of IPBF derivatives were carried out in the recombinant

mouse prion protein (rMoPrP) and brain sections of mouse-adapted bovine spongiform

encephalopathy (mBSE)-infected mice. SPECT imaging of 5-(5-[^{123}I]iodobenzofuran-2-

yl)-*N*-methylpyridin-2-amine ([^{123}I]IPBF-NHMe) was performed on mBSE-infected

and mock-infected mice.

Results: Fluorescence microscopy results showed that fluorescence signals of IPBF

derivatives corresponded to the thioflavin-T positive amyloid deposits of PrP^{Sc} in the

brain sections of mouse-adapted bovine spongiform encephalopathy (mBSE)-infected mice. Among the IPBF derivatives, 5-(5-iodobenzofuran-2-yl)-*N*-methylpyridin-2-amine (IPBF-NHMe) exhibited the highest binding affinity to the recombinant mouse prion protein (rMoPrP) aggregates with a K_i of 14.3 nM. SPECT/computed tomography (CT) imaging and *ex vivo* autoradiography demonstrated that the [123I]IPBF-NHMe distribution in brain tissues of mBSE-infected mice co-localized with PrP[Sc] deposits.

Conclusion: [123I]IPBF-NHMe appears to be a prospective SPECT tracer for monitoring prion deposits in living brain tissues.

Keywords: Prion disease, PrP[Sc], pyridyl benzofuran, single-photon emission computed tomography (SPECT)

1. Introduction

Transmissible spongiform encephalopathies or prion diseases are infectious and lethal transmissible neurodegenerative diseases in both humans and animals [1-3]. Human prion diseases are categorized into the following subtypes: Creutzfeldt-Jakob disease (CJD), Gerstmann-Strauss-Rhinker syndrome (GSS), fatal familial insomnia (FFI), and Kuru. Bovine spongiform encephalopathy (BSE) in cows and chronic wasting disease

(CWD) in deer are known prion diseases of animals [4-7]. Neuropathologic features of these diseases include abnormal accumulation of prion proteins in the brain, cavernous vacuolization, and severe neuronal loss [8]. A unique feature of prion diseases is that they are caused by infectious and/or endogenous factors. Misfolding of the normal cellular prion protein (PrP^C) into the pathogenic scrapie form (PrP^{Sc}) is believed to play an important role in disease progression [9, 10]. PrP^C is a cell surface glycoprotein enriched in α-helical structures, whereas PrP^{Sc} shows an abundance of β-sheets and the ability propagate by seeded protein misfolding [11]. Infiltration of PrP^{Sc} into the body dysregulates calcium homeostasis and initiates the unfolded protein response, which leads to neuronal dysfunction and apoptosis [12]. Furthermore, infectious PrP^{Sc} activates the p38 mitogen-activated protein kinase pathway and subsequent neurodegeneration [13]. However, the detailed molecular mechanism of prion disease is not well understood. The unequivocal diagnosis of prion disease relies on the detection of PrP^{Sc} in postmortem brain tissue [14]. A novel method based on the PrP^{Sc} amplification assay, called real-time quaking-induced conversion (RT-QUIC), enables detection of PrP^{Sc} in the cerebrospinal fluid, olfactory mucosa, and in patients suspected to have prion disease, with extremely high sensitivity and specificity. Recently, RT-QUIC was used for the diagnosis of sporadic CJD [15-17]. Non-invasive imaging techniques such as single-photon emission computed

tomography (SPECT) and positron emission tomography (PET) can help visualize various disorders of the CNS, including prion deposits in the brain [18, 19]. One of the neuropathological features of prion disease is amyloid plaque deposits in the brain consisting of PrP^{Sc}. Therefore, visualization of PrP^{Sc} deposits in the living human brain could help localize the PrP^{Sc} plaques as well as monitor prion disease progression and its manifestations. As PrP^{Sc} has high β-sheet content, similar to beta-amyloid (Aβ) plaques that are characteristic of Alzheimer's disease [20], amyloid imaging probes have been used to visualize PrP^{Sc} in patients with prion disease [21]. However, the PET imaging agents for Aβ, [^{11}C]PIB and [^{11}C]BF-227, failed to detect deposits in patients with GSS and CJD, respectively [22, 23]. Recently, we developed a series of radioligands, including flavonoids [24-27], quinacrines [28, 29], and benzofuran [30, 31], as new prion imaging probes (Fig. 1). Among them, [^{123}I]SC-OMe, one of the styrylchromone derivatives, appeared to be a potential candidate for visualization of prion deposits in mouse-adapted bovine spongiform encephalopathy (mBSE)-infected mice using a small animal SPECT/CT imaging system [26]. However, continued efforts to develop new imaging probes with improved brain distribution and binding affinity are required for clearer PrP^{Sc} and PrP^{Sc}-specific imaging.

Recently, we identified iodinated benzofuran (IBF) derivatives as potent binders of

PrP^{Sc}. Especially, [^{125}I]5-IBF-NHMe displayed an excellent binding affinity for recombinant mouse prion protein (rMoPrP) aggregates with an equilibrium dissociation constant (K_d) of 12.3 nM. However, the brain distribution of IBF derivatives has to be optimized for *in vivo* imaging of PrP^{Sc} [30]. Iodinated pyridyl benzofuran (IPBF) derivatives, in which the benzene ring of IBF is replaced by a pyridine ring, displayed a strong affinity for amyloid plaques such as Aβ and amylin (Fig. 2) [32, 33]. Recently, we have reported that IBF derivatives showed a high affinity for both PrP^{Sc} and Aβ [30]. Since PrP^{Sc} forms a similar β-sheet structure, the IPBF backbone could also be used to develop PrP^{Sc} imaging probes. A central nervous system multiparameter PET optimization (CNS PET MPO) algorithm has been reported for the design and selection of useful CNS PET agents [34, 35]. We have used this algorithm to discuss the *in vivo* results in a recent report on SPECT imaging agents [30]. This method uses a set of six parameters, including ClogP (calculated logP), ClogD (calculated distribution coefficient at pH = 7.4), molecular weight (MW), topological polar surface area (TPSA), number of hydrogen bond donors (HBD), and pKa (ionization constant of the most basic center) as important factors for CNS PET agents. In this algorithm, the desirable ranges were set as ClogP ≤ 2.8, ClogD ≤ 1.7, MW ≤ 305.3, 44.8 < TPSA ≤ 63.3, HBD ≤ 1, and pKa ≤ 7.2. The scores for each parameter can be calculated ranging from 0.0 to 1.0 and most of the

successful CNS PET tracers in the previous data set have CNS PET MPO scores >3 [34].

Table 1 shows the prediction results of IPBF and IBF derivatives which indicated that the

TPSA values of IPBF are more desirable than those of the IBF derivatives. Although only

IPBF-NH$_2$ has a CNS PET MPO score above 3 among the IPBF derivatives, the scores

of IPBF derivatives tend to be higher than those of IBF. In fact, IPBF derivatives showed

superior pharmacokinetics in the brain tissues in comparison to IBF [30, 32]. Therefore,

we speculated that IPBF derivatives could be applied as useful *in vivo* imaging agents for

PrP^{Sc}. Herein, we report feasibility studies on IPBF derivatives as SPECT imaging agents

for PrP^{Sc} via competitive binding assays using rMoPrP aggregates, fluorescence imaging

of brain tissues of mBSE-infected mice, and SPECT studies of mBSE-infected mice.

2. Materials and methods

2.1. General information

All reagents were commercial products and were used without further purification,

unless otherwise indicated. Na^{125}I was purchased from either Muromachi Yakuhin (Tokyo,

Japan) or PerkinElmer Life Sciences Inc. (Boston, MA, USA). High-performance liquid

chromatography (HPLC) analysis and purification were performed using a Shimadzu HPLC system (LC-10AT pump with SPD-10A UV detector, $\lambda = 254$ nm). An automated gamma counter with a NaI(Tl) detector (2470 WIZARD[2], PerkinElmer, MA, USA) was used to measure the radioactivity. 5-[^{125}I]Iodo-2-(4-methylaminophenyl)benzofuran ([^{125}I]5-IBF-NHMe), 5-(5-Iodobenzofuran-2-yl)pyridin-2-amine (IPBF-NH$_2$), 5-(5-Iodobenzofuran-2-yl)-*N*-methylpyridin-2-amine (IPBF-NHMe), [^{123}I]IPBF-NHMe, and 5-(5-Iodobenzofuran-2-yl)-*N*,*N*-dimethylpyridin-2-amine (IPBF-NMe$_2$) were prepared according to the literature [30, 32].

2.2. Competitive binding assay using rMoPrP aggregates

Expression and aggregation of rMoPrP were performed as described previously [15, 36, 37]. Binding assays for IPBF derivatives and rMoPrP aggregates were performed according to our previous study [30]. Briefly, the mixture contained [^{125}I]5-IBF-NHMe (0.02 nM), test compound (4.0 pM−1.0 μM), and rMoPrP aggregates (100 nM) in the assay buffer. After incubation for 2 h at room temperature, the mixture was filtered and the filtrates quantified using a gamma counter. Nonspecific binding was measured in the presence of 10 μM non-radioactive 5-IBF-NHMe. Values for the half maximal inhibitory

concentration (IC_{50}) were determined from displacement curves of three independent experiments using PRISM4, and those for the K_i were calculated using the Cheng–Prusoff equation.

2.3. Animals

All animals used in the study were supplied by Kyudo Co., Ltd. (Saga, Japan). Experiments that involved infecting animals with mBSE were conducted in conformance with biosafety level 3 (BSL3) containment in accordance with institutional guidelines. The mBSE-infected and mock-infected mice were treated as previously reported [38, 39]. To prepare the mBSE-infected mice, mBSE was serially passaged into ddY mice by intracerebral inoculation. Experiments using animals were conducted in accordance with our institutional guidelines and were approved by the Nagasaki University Animal Care Committee (Approval number; 1211201033-5).

2.4. Fluorescence staining of mBSE-infected and mock-infected mouse brain sections

The animals used for the *in vitro* experiments were exsanguinated *via* transcardial

perfusion using saline under isoflurane anesthesia. Their brains were subsequently

excised and frozen using an ethanol (EtOH) ice bath. Frozen blocks were sliced into 10

µm serial sections and incubated with a 20% DMSO solution containing IPBF derivatives

(100 µM) for 24 h. Each section was washed twice with 20% DMSO. Fluorescence

images were obtained using an Eclipse 80i microscope (Nikon Corp., Tokyo, Japan) with

a B-2A filter set (excitation: 450–490 nm; dichromic mirror: 505 nm; longpass filter:

520 nm). The PrP^{Sc} deposits in the serial sections were detected using fluorescence

staining with Thioflavin T (ThT, 50 µM) [26, 29].

2.5. Small-animal SPECT/CT imaging of mBSE-infected mice

SPECT/CT imaging studies of mBSE-infected mice (ddY, 23–25 weeks old, male,

38.4–45.9 g, n = 5) or mock-infected mice (ddY, 25–26 weeks old, male, 32.1–40.1 g)

were performed using the Triumph combined PET/SPECT/CT systems (TriFoil Imaging

Inc., CA, USA). Each mouse was administered [^{123}I]IPBF-NHMe (53.6−80.4 MBq) via

tail vein injection. Immediately after injection, the mice were anesthetized using 1.5%

(v/v) isoflurane. SPECT imaging was performed with a four-head γ-camera equipped with

single pinhole collimators (diameter: 1.0 mm; focal length: 90 mm). SPECT data was

acquired for 33 min (radius of rotation: 40 mm; rotation angle: 360°; projection number: 64; time per projection: 30 s) starting at 20 min after intravenous injection. SPECT imaging was followed by CT image acquisition (X-ray source: 60 kV; 128 projections), with animals maintained in exactly the same position. The SPECT data was reconstructed using a 3D-Maximum-Likelihood Expectation Maximization (3D-MLEM) algorithm with 50 iterations and the SPECT/CT images were prepared using the OsiriX MD software (Pixmeo, Geneva, Switzerland). After SPECT/CT imaging, the mouse was sacrificed and the entire brain frozen on dry ice/ EtOH baths, followed by the preparation of coronal sections (10 μm) using a cryostat microtome. Thereafter, the images of immunohistochemical staining of PrP^{Sc} and autoradiograms for radioactivity in the brain sections were obtained using the methods described above. After autoradiography analysis, the tissues were washed with 50% (v/v) EtOH and autoclaved in 1.2 mM HCl at 121 °C for 10 min and then treated with formic acid for 15 min. After blocking with 0.3% (v/v) H_2O_2 for 30 min, normal goat serum (1:20) was added for 30 min. The tissues were incubated overnight with the SAF32 anti-PrP antibody (1:20). After washing with Tris-HCl buffer (pH 7.5) containing 0.05% (v/v) Tween 20, the tissue sections were incubated with a secondary anti-mouse biotinylated antibody for 1.5 h. Fluorescence signals were visualized by reaction with hydrogen peroxidase-activated

diaminobenzidine.

3. Results and discussion

3.1. *In vitro* binding of IPBF derivatives to rMoPrP aggregates

In our previous studies, we used rMoPrP aggregates as PrP^{Sc} models to screen efficient prion imaging probes [26, 29]. It is reported that the recombinant PrP of various species, including rMoPrP and recombinant human PrP (rHuPrP), show aggregation patterns different from each other [40, 41]. Both recombinant PrP (rPrP) alone and rPrP seeded with PrP^{Sc} form β-sheet-rich aggregates with intermittent shaking [15, 37]. Fluorescence of Th-T, FTIR, and electron microscopy confirmed that the PrP^{Sc} aggregates mainly consisted of amyloid-like fibrils as deposits in the brain tissue of patients with prion disease [37]. We have previously examined the optimized aggregation model using rMoPrP. Because aggregates prepared from MoPrP alone had the highest percentage of β-sheets they were used for subsequent evaluation (data not shown). Since [^{125}I]5-IBF-NHMe showed the highest binding affinity (K_d = 12.3 nM) for rMoPrP aggregates among the series of prion imaging probes tested [26, 29, 30], the inhibition constant (K_i) values

of non-radioactive IPBF derivatives for rMoPrP aggregates were evaluated using displacement studies of [^{125}I]5-IBF-NHMe. As shown in Table 2, the IPBF derivatives showed high affinities for rMoPrP aggregates in the order IPBF-NHMe (K_i = 14.3 nM) > IPBF-NMe$_2$ (Ki = 16.7 nM) > IPBF-NH$_2$ (K_i = 60.4 nM). All IPBF derivatives exhibit strong binding affinities for Aβ$_{1-42}$ aggregates, which ranged from a K_i of 2.4 to 10.3 nM. In addition, IPBF-NMe$_2$ showed high binding affinity for amylin aggregates (K_d= 8.31 nM) [33]. This suggests that IPBF derivatives recognize broad amyloid conformations with strong binding affinities. There are slight differences in binding properties between PrP^{Sc} and Aβ. The compounds showing the strongest affinity for PrP^{Sc} and Aβ were IPBF-NHMe and IPBF-NMe$_2$, respectively. As binding affinities of IPBF-NHMe and 5-IBF-NHMe for PrP^{Sc} are comparable, converting the benzene ring at the 3-position of benzofurans into a pyridine ring appears to have no effect on the affinity for PrP^{Sc}. Similar to Aβ, the introduction of NH$_2$ in the benzene ring reduced the affinity for PrP^{Sc}. The rMoPrP showed different aggregation patterns with recombinant human PrP (rHuPrP) [15]. We have used only rMoPrP aggregates in this study because rMoPrP quickly forms β-sheet-rich aggregates, making them easy to use in initial binding studies. Even using rHuPrP aggregates to screen the prion imaging probes, protein aggregation models may have limitation to predict clinical results.

3.2. Fluorescence staining of IPBF derivatives in mBSE-infected mouse brain sections

Next, we performed neuropathological fluorescence staining of IPBF derivatives

in brain sections from mBSE- and mock-infected mice. To identify amyloid aggregates

in the mouse brain slices, we used ThT, a well-known amyloid-staining dye that can detect

PrP^{Sc} [42, 43]. Distinct fluorescence signals were obtained for IPBF-NH$_2$, IPBF-NHMe,

and IPBF-NMe$_2$ (Fig. 3A, B, and C, respectively) in mBSE-infected mouse brain sections,

which co-localized with the ThT staining pattern in the adjacent brain sections (Fig. 3D,

E, and F, respectively). However, no significant fluorescence signals from IPBF-NH$_2$,

IPBF-NHMe, and IPBF-NMe$_2$ were observed in brain sections of age-matched mock-

infected mice (Fig. 3G, H, and I, respectively) in which no PrP^{Sc} deposits were detected

in brain tissue sections (Fig. 3J, K, and L, respectively). These results suggested that these

three IPBF derivatives recognize deposits consisting of PrP^{Sc} in the mBSE-infected

mouse brain despite their varying affinities for rMoPrP aggregates. Next, we performed

additional fluorescence imaging of IPBF-NHMe in the brain sections of mBSE- and

mock-infected mice with immunohistochemical staining for PrP^{Sc} of the adjacent brain

sections using an anti-PrP antibody. As shown in Fig. 4A and B, we confirmed co-

localization of IPBF-NHMe with the antibody-labeled PrP deposits. Mock-infected mice

showed no significant signal of IPBF-NHMe, which was also consistent with the absence

of PrP^{Sc} in the brain tissue (Fig. 4C and D).

3.3. Small-animal SPECT/CT imaging studies of [^{123}I]IPBF-NHMe

IPBF-NHMe had the highest binding affinity for rMoPrP aggregates among the IPBF

derivatives used in this study (Table 1). Furthermore, a previous study demonstrated that

[^{125}I]IPBF-NHMe showed high initial uptake in the brain [4.17% injected dose (ID)/g at

2 min post-injection] and favorable washout from normal brain tissues (1.30 % ID/g at

60 min post-injection) [32]. The $brain_{2\ min}/brain_{60\ min}$ ratio in the normal mouse brain is

often used as an index parameter to compare the washout rate among amyloid imaging

probes. The $brain_{2min}/brain_{60min}$ ratio of [^{125}I]IPBF-NHMe is 3.2 [32], which is

comparable with that of clinically useful probes [^{18}F]Florbetapir (3.8) [44] and

[^{18}F]Florbetaben (4.8) [45]. Therefore, we selected IPBF-NHMe for small-animal SPECT

studies in mBSE- and mock-infected mouse brains to validate their potential as *in vivo*

imaging agents for detection of prion deposits in the brain. For SPECT imaging,

[^{123}I]IPBF-NHMe was synthesized according to a previous report [32] with radiochemical

yields of 51–66% and a radiochemical purity of >98% (data not shown). Representative composite SPECT/CT images of [^{123}I]IPBF-NHMe from 20 to 60 min are shown in Figures 4A and 4B, respectively. Use of [^{123}I]IPBF-NHMe demonstrated that its distribution was quite different between mBSE-infected and mock-infected mice. High levels of [^{123}I]IPBF-NHMe in the corpus callosum and thalamus of the mBSE-infected brain were clearly visualized (Fig. 5A). On the other hand, no significant [^{123}I]IPBF-NHMe signals were observed in age-matched mock-infected brains (Fig. 5B). After SPECT imaging, *ex vivo* autoradiography of dissected brain sections demonstrated significant [^{123}I]IPBF-NHMe accumulation in the mBSE-infected mouse brain (Fig. 5C), whereas, low [^{123}I]IPBF-NHMe binding was observed in mock-infected mouse brains (Fig. 5D). The precise site of PrP^{Sc} deposition in the mouse model depends on the individual. In fact, our previous research demonstrated the presence of high levels of PrP^{Sc} in the right hemisphere including the cerebral cortex, hippocampus, and corpus callosum of the brain tissues from mBSE-infected mice. In this study, regions showing high accumulation of [^{123}I]IPBF-NHMe in the corpus callosum and thalamus of mBSE-infected brains were confirmed to be PrP^{Sc}-positive using immunohistochemical analysis (Fig. 5E and F, respectively), whereas, no PrP^{Sc} deposits were detected in mock-infected brains (Fig. 5H and I, respectively). These results indicated that [^{123}I]IPBF-NHMe could

be a prospective SPECT imaging probe for cerebral prion deposits, an instrument for investigation of prion diseases, and as a tool for the development of therapeutic agents for prion diseases both in basic research and clinical studies. Nevertheless, it should be taken into consideration that IPBF derivatives have high binding affinities not only for rMoPrP but also for other amyloids including Aβ [32] and amylin [33]. Although, there are few reports of CJD with AD symptoms, PrP deposits were observed at the Aβ plaques in the cerebral cortex of coexistence of sCJD patients with AD pathology [46, 47]. In GSS patients, numerous PrP^{Sc} and Aβ deposits were simultaneously present in the cerebral cortex. Both, PrP^{Sc} and Aβ were detected in the thalamuses of patients with sCJD and familial Alzheimer's disease, respectively [48-50]. Notably, several reports have shown strong PrP^{Sc} deposition in the cerebellum of CJD patients [49, 51]. Similarly, PrP^{Sc} deposition was detected in the cerebellum; however, Aβ deposition was not observed therein in GSS patients [52]. The appearance of Aβ deposits in the neocortex began at an early stage, whereas, deposits in the cerebellum were detected only at the end of AD patients [53]. Given these reports, the detection of amyloid plaques in the cerebellum with non-selective amyloid imaging probes may, in some cases, facilitate the differential diagnosis between GSS and other amyloid disorders. However, using amyloid selective imaging probes is considered desirable to accurately distinguish between prion diseases

and AD. As IPBF derivatives exhibit an excellent binding affinity for PrP^{Sc} with selective

brain distribution favorable for *in vivo* imaging, IPBF scaffolds may be useful for further

development of PrP^{Sc}-specific imaging probes. Previously, we used rMoPrP and mBSE-

infected mice to screen imaging probes for PrP^{Sc}. We found consistent binding properties

of these compounds during binding affinity determination using rMoPrP, *in vitro*

fluorescence, and autoradiography binding in the brain sections from mBSE-infected

mice, and SPECT imaging of mBSE-infected mice [26, 30]. Therefore, we used these

models for the initial feasibility study of IPBF derivatives for screening useful imaging

probes in this study. The mBSE model used in this study has detected PrP^{Sc} in primary

cultured bone marrow stromal cells as shown in the those collected from patients with

sCJD. The mBSE-infected mice showed abnormal gait and other neurological signs as

common characteristics of prion disease [54]. Therefore, it is considered to be a suitable

model in which pathological conditions similar to human clinical symptoms occur.

However, mBSE-infected mice lack human PrP and may be dissociated from the

pathology of a high proportion of prion diseases such as sCJD. Further preclinical

evaluation using various animal models of prion diseases such as sCJD prion-inoculated

mice expressing humanized PrP [55] and clinical SPECT studies of patients with prion

disease are necessary to assess [^{123}I]IPBF-NHMe as a clinically useful prion imaging

probe in the future.

4. Conclusion

We performed feasibility studies of IPBF derivatives as prion imaging probes. [^{125}I]IPBF-NHMe exhibited the highest binding affinity for rMoPrP aggregates among the IPBF derivatives evaluated in this study. Additionally, fluorescence imaging with IPBF-NHMe was used to detect PrP^{Sc} deposits in mBSE-infected mouse brain tissues. Crucially, [^{123}I]IPBF-NHMe allowed visualization of prion deposits in mBSE-infected mice using small animal SPECT/CT imaging systems. Thus, [^{123}I]IPBF-NHMe could be a potential SPECT imaging probe for visualization of PrP^{Sc} in living brain tissues.

Declaration of competing interest

The authors declare that they have no conflicts of interest

Acknowledgements

Reference

[1] Collinge J. Mammalian prions and their wider relevance in neurodegenerative diseases. Nature 2016;539:217-26.

[2] Prusiner SB. Prions. Proceedings of the National Academy of Sciences of the United States of America 1998;95:13363-83.

[3] Walker LC and Jucker M. Neurodegenerative Diseases: Expanding the Prion Concept. Annual Review of Neuroscience; 2015, p. 87-103.

[4] Aguilar-Calvo P, García C, Espinosa JC, Andreoletti O, and Torres JM. Prion and prion-like diseases in animals. Virus research 2015;207:82-93.

[5] Aguzzi A and Calella AM. Prions: protein aggregation and infectious diseases. Physiological reviews 2009;89:1105-52.

[6] Houston F and Andréoletti O. Animal prion diseases: the risks to human health. Brain pathology (Zurich, Switzerland) 2019;29:248-62.

[7] Watts JC, Balachandran A, and Westaway D. The expanding universe of prion diseases. PLoS pathogens 2006;2:e26.

[8] Budka H. Neuropathology of prion diseases. British medical bulletin 2003;66:121-30.

[9] AM TI, Adlard PA, Finkelstein DI, Lewis V, Biggi S, Biasini E, et al. Acute Neurotoxicity Models of Prion Disease. ACS Chem Neurosci 2018;9:431-45.

[10] Soto C and Pritzkow S. Protein misfolding, aggregation, and conformational strains in neurodegenerative diseases. Nature neuroscience 2018;21:1332-40.

[11] Requena JR. The protean prion protein. PLoS biology 2020;18:e3000754.

[12] Shah SZA, Zhao D, Hussain T, and Yang L. The Role of Unfolded Protein Response and Mitogen-Activated Protein Kinase Signaling in Neurodegenerative Diseases with Special Focus on Prion Diseases. Frontiers in aging neuroscience 2017;9:120.

[13] Puig B, Altmeppen HC, and Glatzel M. Misfolding leads the way to unraveling signaling pathways in the pathophysiology of prion diseases. Prion 2016;10:434-43.

[14] Puoti G, Bizzi A, Forloni G, Safar JG, Tagliavini F, and Gambetti P. Sporadic human prion diseases: molecular insights and diagnosis. The Lancet. Neurology 2012;11:618-28.

[15] Atarashi R, Satoh K, Sano K, Fuse T, Yamaguchi N, Ishibashi D, et al. Ultrasensitive human prion detection in cerebrospinal fluid by real-time quaking-induced conversion. Nature medicine 2011;17:175-8.

[16] Bongianni M, Orrù C, Groveman BR, Sacchetto L, Fiorini M, Tonoli G, et al. Diagnosis of human prion disease using real-time quaking-induced conversion testing of olfactory mucosa and cerebrospinal fluid samples. JAMA Neurology 2017;74:155-62.

[17] Zerr I and Parchi P. Sporadic Creutzfeldt-Jakob disease. Handbook of clinical neurology 2018;153:155-74.

[18] Fuchigami T. [Development of Molecular Probes for Live Imaging of Cancer and Infectious Diseases]. Yakugaku zasshi : Journal of the Pharmaceutical Society of Japan 2019;139:1531-8.

[19] Ono M. Development of positron-emission tomography/single-photon emission computed tomography imaging probes for in vivo detection of beta-amyloid plaques in Alzheimer's brains. Chemical & pharmaceutical bulletin 2009;57:1029-39.

[20] Rambaran RN and Serpell LC. Amyloid fibrils: abnormal protein assembly. Prion 2008;2:112-7.

[21] Letourneau-Guillon L, Wada R, and Kucharczyk W. Imaging of prion diseases. Journal of magnetic resonance imaging : JMRI 2012;35:998-1012.

[22] Deters KD, Risacher SL, Yoder KK, Oblak AL, Unverzagt FW, Murrell JR, et al. [(11)C]PiB PET in Gerstmann-Straussler-Scheinker disease. American journal of nuclear medicine and molecular imaging 2016;6:84-93.

[23] Okamura N, Shiga Y, Furumoto S, Tashiro M, Tsuboi Y, Furukawa K, et al. In vivo detection of prion amyloid plaques using [(11)C]BF-227 PET. European journal of nuclear medicine and molecular imaging 2010;37:934-41.

[24] Fuchigami T, Ogawa A, Yamashita Y, Haratake M, Watanabe H, Ono M, et al. Development of alkoxy styrylchromone derivatives for imaging of cerebral amyloid-β plaques with SPECT. Bioorganic and Medicinal Chemistry Letters 2015;25:3363-7.

[25] Fuchigami T, Yamashita Y, Haratake M, Ono M, Yoshida S, and Nakayama M. Synthesis and evaluation of ethyleneoxylated and allyloxylated chalcone derivatives for imaging of amyloid β plaques by SPECT. Bioorganic and Medicinal Chemistry 2014;22:2622-8.

[26] Fuchigami T, Yamashita Y, Kawasaki M, Ogawa A, Haratake M, Atarashi R, et al. Characterisation of radioiodinated flavonoid derivatives for SPECT imaging of cerebral prion deposits. Scientific Reports 2015;5.

[27] Ono M, Ikeoka R, Watanabe H, Kimura H, Fuchigami T, Haratake M, et al. Synthesis and evaluation of novel chalcone derivatives with 99mTc/Re complexes as potential probes for detection of β-amyloid plaques. ACS Chemical Neuroscience 2010;1:598-607.

[28] Fuchigami T, Kobashi N, Haratake M, Kawasaki M, and Nakayama M. Synthesis and biological evaluation of radioiodinated quinacrine-based derivatives for SPECT

imaging of Aβ plaques. European Journal of Medicinal Chemistry 2013;60:469-78.

[29] Kawasaki M, Fuchigami T, Kobashi N, Nakagaki T, Sano K, Atarashi R, et al. Development of radioiodinated acridine derivatives for in vivo imaging of prion deposits in the brain. Bioorganic and Medicinal Chemistry 2017;25:1085-93.

[30] Fuchigami T, Kawasaki M, Koyama R, Nakaie M, Nakagaki T, Sano K, et al. Development of Radioiodinated Benzofuran Derivatives for in Vivo Imaging of Prion Deposits in the Brain. ACS infectious diseases 2019.

[31] Ono M, Fuchi Y, Fuchigami T, Kobashi N, Kimura H, Haratake M, et al. Novel benzofurans with 99mTc complexes as probes for imaging cerebral β-amyloid plaques. ACS Medicinal Chemistry Letters 2010;1:443-7.

[32] Ono M, Cheng Y, Kimura H, Watanabe H, Matsumura K, Yoshimura M, et al. Development of Novel 123I-Labeled Pyridyl Benzofuran Derivatives for SPECT Imaging of β-Amyloid Plaques in Alzheimer's Disease. PloS one 2013;8:e74104.

[33] Yoshimura M, Ono M, Watanabe H, Kimura H, and Saji H. Feasibility of Amylin Imaging in Pancreatic Islets with β-Amyloid Imaging Probes. Scientific Reports 2014;4:6155.

[34] Zhang L, Villalobos A, Beck EM, Bocan T, Chappie TA, Chen L, et al. Design and selection parameters to accelerate the discovery of novel central nervous system positron

emission tomography (PET) ligands and their application in the development of a novel

phosphodiesterase 2A PET ligand. J Med Chem 2013;56:4568-79.

[35] Wager TT, Hou X, Verhoest PR, and Villalobos A. Moving beyond rules: the

development of a central nervous system multiparameter optimization (CNS MPO)

approach to enable alignment of druglike properties. ACS Chem Neurosci 2010;1:435-

49.

[36] Atarashi R, Moore RA, Sim VL, Hughson AG, Dorward DW, Onwubiko HA, et al.

Ultrasensitive detection of scrapie prion protein using seeded conversion of recombinant

prion protein. Nature methods 2007;4:645-50.

[37] Sano K, Atarashi R, Ishibashi D, Nakagaki T, Satoh K, and Nishida N.

Conformational properties of prion strains can be transmitted to recombinant prion

protein fibrils in real-time quaking-induced conversion. Journal of virology

2014;88:11791-801.

[38] Fujihara A, Atarashi R, Fuse T, Ubagai K, Nakagaki T, Yamaguchi N, et al.

Hyperefficient PrP Sc amplification of mouse-adapted BSE and scrapie strain by protein

misfolding cyclic amplification technique. The FEBS journal 2009;276:2841-8.

[39] Nakagaki T, Satoh K, Ishibashi D, Fuse T, Sano K, Kamatari YO, et al. FK506

reduces abnormal prion protein through the activation of autolysosomal degradation and

prolongs survival in prion-infected mice. Autophagy 2013;9:1386-94.

[40] Ubagai K, Fukuda S, Mori T, Takatsuki H, Taguchi Y, Kageyama S, et al. Discrimination between L-type and C-type bovine spongiform encephalopathy by the strain-specific reactions of real-time quaking-induced conversion. Biochemical and biophysical research communications 2020;526:1049-53.

[41] Masujin K, Orrú CD, Miyazawa K, Groveman BR, Raymond LD, Hughson AG, et al. Detection of Atypical H-Type Bovine Spongiform Encephalopathy and Discrimination of Bovine Prion Strains by Real-Time Quaking-Induced Conversion. Journal of clinical microbiology 2016;54:676-86.

[42] Polano M, Bek A, Benetti F, Lazzarino M, and Legname G. Structural insights into alternate aggregated prion protein forms. J Mol Biol 2009;393:1033-42.

[43] Hervé R, Collin R, Pinchin HE, Secker T, and Keevil CW. A rapid dual staining procedure for the quantitative discrimination of prion amyloid from tissues reveals how interactions between amyloid and lipids in tissue homogenates may hinder the detection of prions. Journal of microbiological methods 2009;77:90-7.

[44] Zhang W, Oya S, Kung MP, Hou C, Maier DL, and Kung HF. F-18 Polyethyleneglycol stilbenes as PET imaging agents targeting Abeta aggregates in the brain. Nuclear medicine and biology 2005;32:799-809.

[45] Zhang W, Kung MP, Oya S, Hou C, and Kung HF. 18F-labeled styrylpyridines as PET agents for amyloid plaque imaging. Nuclear medicine and biology 2007;34:89-97.

[46] Haraguchi T, Terada S, Ishizu H, Sakai K, Tanabe Y, Nagai T, et al. Coexistence of Creutzfeldt-Jakob disease, Lewy body disease, and Alzheimer's disease pathology: an autopsy case showing typical clinical features of Creutzfeldt-Jakob disease. Neuropathology : official journal of the Japanese Society of Neuropathology 2009;29:454-9.

[47] Tsuchiya K, Yagishita S, Ikeda K, Sano M, Taki K, Hashimoto K, et al. Coexistence of CJD and Alzheimer's disease: an autopsy case showing typical clinical features of CJD. Neuropathology : official journal of the Japanese Society of Neuropathology 2004;24:46-55.

[48] Aggleton JP, Pralus A, Nelson AJ, and Hornberger M. Thalamic pathology and memory loss in early Alzheimer's disease: moving the focus from the medial temporal lobe to Papez circuit. Brain : a journal of neurology 2016;139:1877-90.

[49] Iwasaki Y, Hiraga K, Ito S, Ando T, Akagi A, Riku Y, et al. Autopsy case of MV2K-type sporadic Creutzfeldt-Jakob disease with spongiform changes of the cerebral cortex. Neuropathology : official journal of the Japanese Society of Neuropathology 2019;39:452-60.

[50] Kobayashi A, Iwasaki Y, Takao M, Saito Y, Iwaki T, Qi Z, et al. A Novel Combination of Prion Strain Co-Occurrence in Patients with Sporadic Creutzfeldt-Jakob Disease. Am J Pathol 2019;189:1276-83.

[51] Monzón M, Hernández RS, Garcés M, Sarasa R, and Badiola JJ. Glial alterations in human prion diseases. Medicine (United States) 2018;97.

[52] Ishizawa K, Mitsufuji T, Shioda K, Kobayashi A, Komori T, Nakazato Y, et al. An autopsy report of three kindred in a Gerstmann-Straussler-Scheinker disease P105L family with a special reference to prion protein, tau, and beta-amyloid. Brain and behavior 2018;8:e01117.

[53] Thal DR, Rub U, Orantes M, and Braak H. Phases of A beta-deposition in the human brain and its relevance for the development of AD. Neurology 2002;58:1791-800.

[54] Takakura Y, Yamaguchi N, Nakagaki T, Satoh K, Kira J, and Nishida N. Bone marrow stroma cells are susceptible to prion infection. Biochemical and biophysical research communications 2008;377:957-61.

[55] Nakagaki T, Ishibashi D, Mori T, Miyazaki Y, Takatsuki H, Tange H, et al. Administration of FK506 from Late Stage of Disease Prolongs Survival of Human Prion-Inoculated Mice. Neurotherapeutics 2020.

Table 1. Individual CNS PET MPO parameters of IBF and IBPF derivatives.
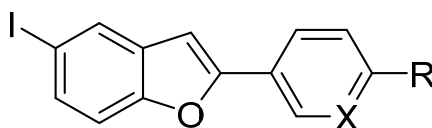
IPBF and IBF derivatives

Compound	R	X	ClogP[a]	ClogD[b]	TPSA[a]	MW	HBD	pKa[b]	CNS PET MPO[c]
IPBF-NH$_2$	NH$_2$	N	3.31	4.40	47.61	336.1	1	4.60	3.8
IPBF-NHMe	NHMe	N	3.61	4.93	33.62	350.2	1	4.61	2.4
IPBF-NMe$_2$	NMe$_2$	N	4.40	5.14	24.83	364.2	1	4.71	2.0
5-IBF-NH$_2$	NH$_2$	CH	3.93	4.57	35.25	335.1	1	3.52	2.6
5-IBF-NHMe	NHMe	CH	4.23	5.02	21.26	349.2	1	3.88	2.0
5-IBF-NMe$_2$	NMe$_2$	CH	5.02	5.42	12.47	363.2	1	4.27	2.0

[a] The physicochemical properties of each compound was calculated using a ChemBioDraw Ultra 13.0.

[b] The physicochemical properties of each compound was calculated using a SPARK on

line calculator.

[c] The CNS PET MPO of each compound was calculated according to the literature [34].

ClogP, calculated partition coefficient; ClogD, calculated distribution coefficient at

pH=7.4; MW, molecular weight; TPSA, topological polar surface area; HBD, number of

hydrogen bond donors, pKa, ionization constant of the most basic center.

Table 2. The K_i values of IPBF and IBF derivatives for rMoPrP, $A\beta_{1-42}$ and amylin

aggregates.
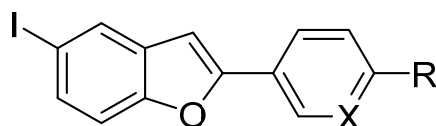
IPBF and IBF derivatives

Compound	R	X	K_i (nM)		
			rMoPrP[a]	$A\beta_{1-42}$	Amylin
IPBF-NH$_2$	NH$_2$	N	60.4 (12.5)	10.3 (1.48)[b]	–
IPBF-NHMe	NHMe	N	14.3 (1.26)	2.94 (0.22)[b]	–
IPBF-NMe$_2$	NMe$_2$	N	16.7 (0.61)	2.36 (0.53)[b]	2.66 (0.55)[d]
5-IBF-NHMe	NHMe	CH	12.1 (1.90)[c]	3.79 (0.15)[c]	–

[a] Data represent the mean ± standard error of the mean for three independent experiments.

[b] Data from ref. [32].

[c] Data from ref. [30].

[d] Data from ref. [33].

FIGURES

Figure 1
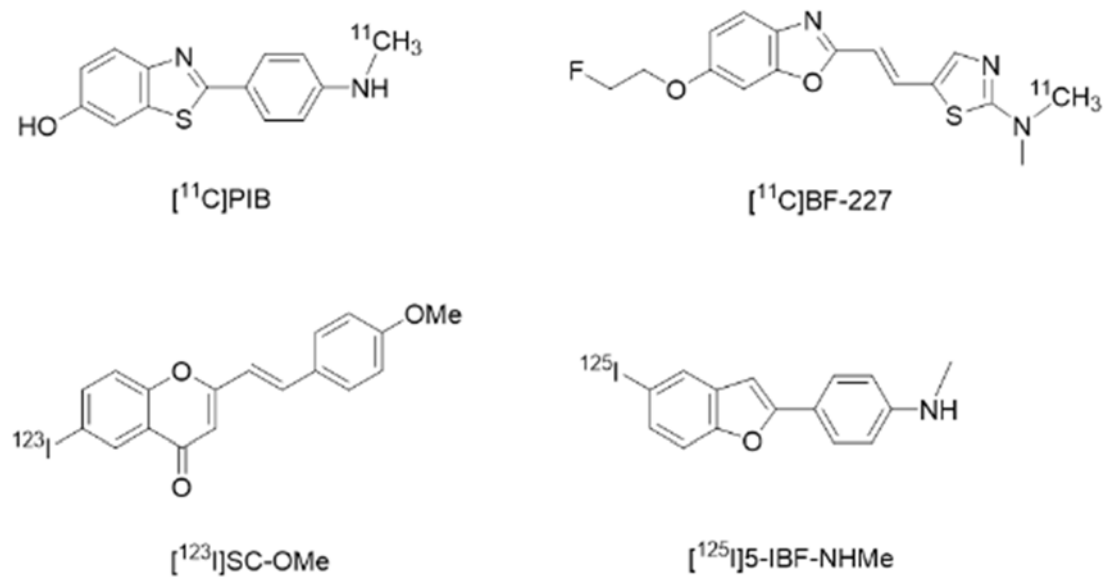
Fig 1. Chemical structures of investigated prion imaging probes.

Figure 2

IPBF-NH₂: R= NH₂, X= I
[¹²³I]IPBF-NHMe: R= NHMe, X= ¹²³I
IPBF-NMe₂: R= NMe₂, X= I

Fig 2. Chemical structures of radioiodinated pyridyl benzofuran derivatives evaluated in

this study.

Figure 3
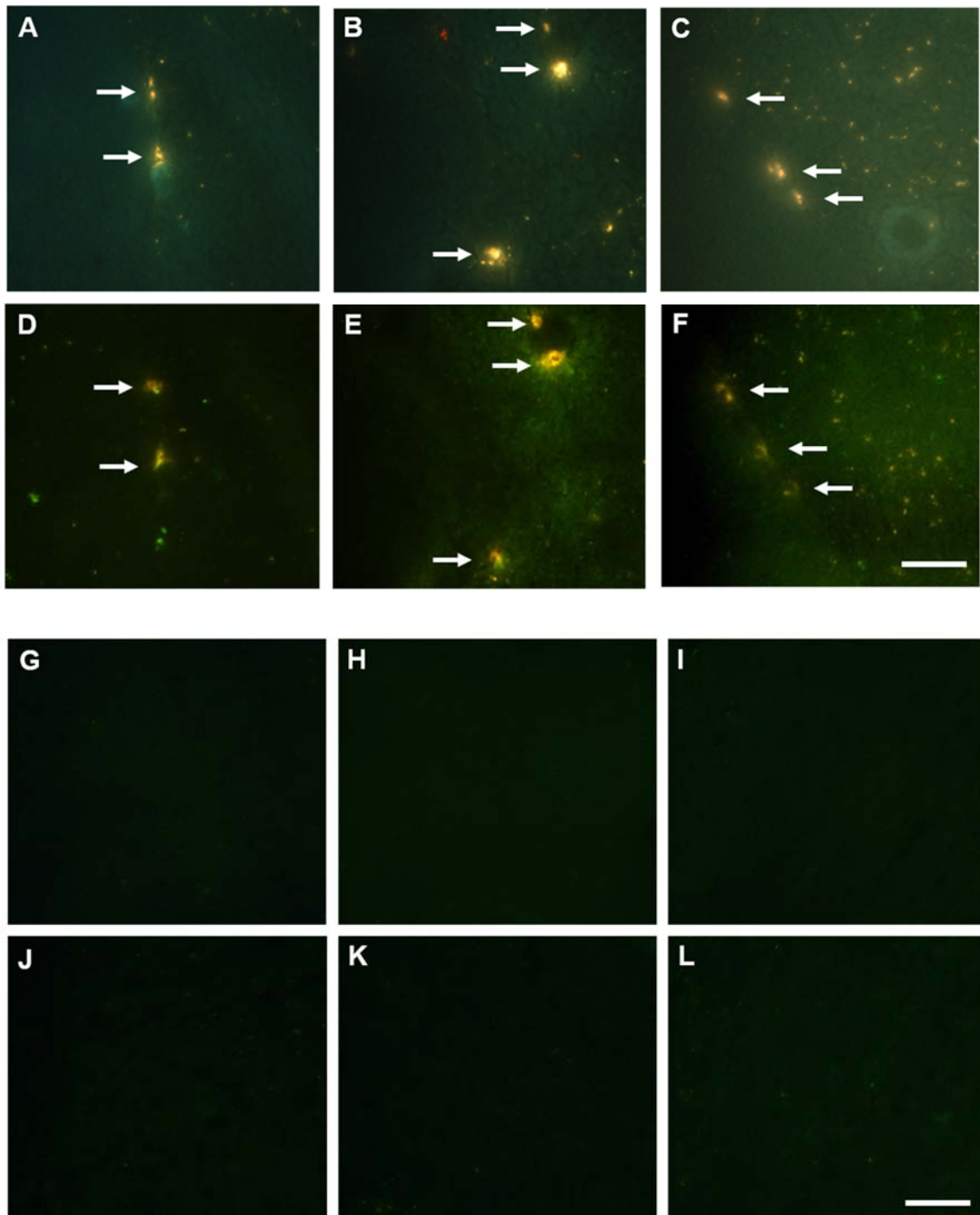
Fig 3. Fluorescence staining of pyridyl benzofuran (IPBF) derivatives (IPBF-NH$_2$, IPBF-NHMe, IPBF-NMe$_2$) in brain sections of mouse-adapted bovine spongiform encephalopathy (mBSE)-infected mice (A–C) and mock-infected mice (G–I), respectively. The adjacent brain sections of mBSE-infected mice (D–F) and mock-infected mice (J–L) were stained with ThT. Scale bar = 50 μm.

Figure 4
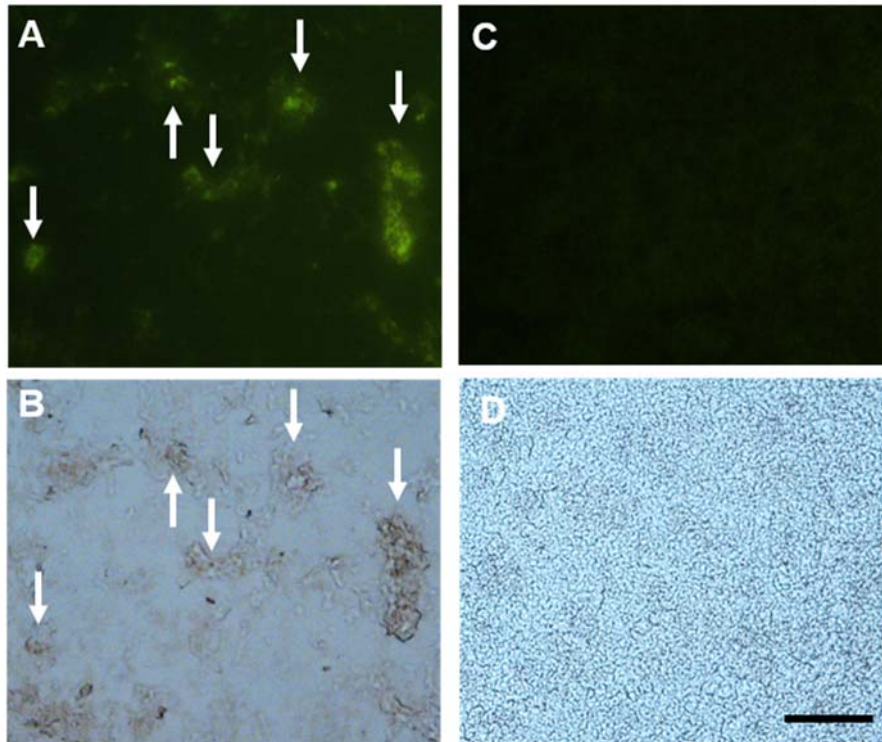
Fig. 4. Fluorescence staining of IPBF-NHMe in the brain sections of mBSE-infected

mice (A) and mock-infected mice (C). Immunohistochemical staining for PrP^{Sc} of

adjacent sections using an anti-PrP antibody (B and D, respectively). Scale bar = 50 μm.

Figure 5
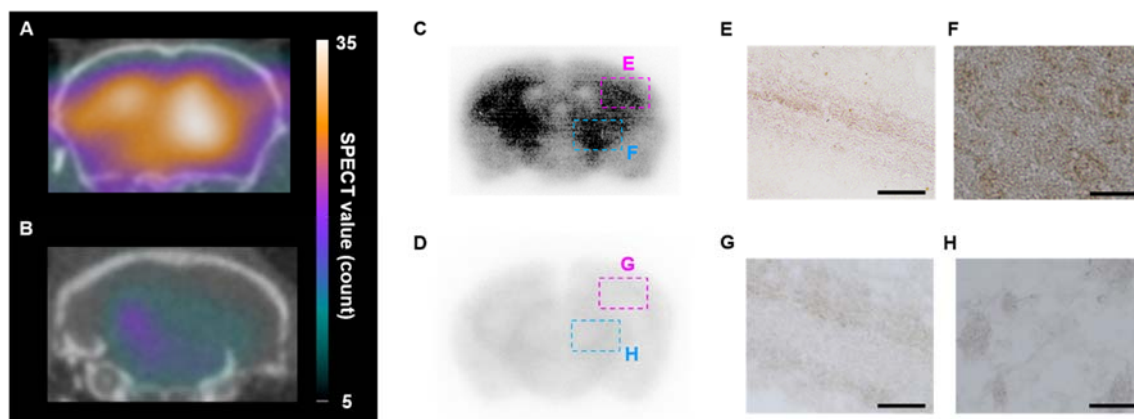
Fig 5. Representative composite SPECT/CT images of mBSE-infected (**A**) and mock-infected mice (**B**) over 20 to 60 min after injection of [^{123}I]IPBF-NHMe. *Ex vivo* autoradiography of corresponding brain slices from the same mBSE-infected (**C**) and mock-infected mice (**D**). Immunohistochemical staining for PrP^{Sc} in corpus callosum (**E** and **G**) and thalamus (**F** and **H**) of mBSE- and mock-infected mouse brain, respectively. Scale bar = 50 μm.